Bi-Sparse Unsupervised Feature Selection

Xianchao Xiu, Member, IEEE, Chenyi Huang, Pan Shang, and Wanquan Liu, Senior Member, IEEE

Abstract—To efficiently deal with high-dimensional datasets in many areas, unsupervised feature selection (UFS) has become a rising technique for dimension reduction. Even though there are many UFS methods, most of them only consider the global structure of datasets by embedding a single sparse regularization or constraint. In this paper, we introduce a novel bi-sparse UFS method, called BSUFS, to simultaneously characterize both global and local structures. The core idea of BSUFS is to incorporate $\ell_{2,p}$ -norm and ℓ_q -norm into the classical principal component analysis (PCA), which enables our proposed method to select relevant features and filter out irrelevant noise accurately. Here, the parameters p and q are within the range of [0,1). Therefore, BSUFS not only constructs a unified framework for bi-sparse optimization, but also includes some existing works as special cases. To solve the resulting non-convex model, we propose an efficient proximal alternating minimization (PAM) algorithm using Riemannian manifold optimization and sparse optimization techniques. Theoretically, PAM is proven to have global convergence, i.e., for any random initial point, the generated sequence converges to a critical point that satisfies the first-order optimality condition. Extensive numerical experiments on synthetic and realworld datasets demonstrate the effectiveness of our proposed BSUFS. Specifically, the average accuracy (ACC) is improved by at least 4.71% and the normalized mutual information (NMI) improved by at least 3.14% on average compared to the existing UFS competitors. The results validate the advantages of bi-sparse optimization in feature selection and show its potential for other fields in image processing. Our code will be available at https://github.com/xianchaoxiu.

Index Terms—Unsupervised feature selection, bi-sparse, principal component analysis (PCA), proximal alternating minimization, Riemannian manifold optimization

I. Introduction

IGH-DIMENSIONAL features make data processing challenging due to the fact that there are lots of redundant information and additional noise [1]. To tackle this challenge, feature selection techniques are proposed and studied to select important features. One can read the review paper [2] for more comprehensive backgrounds and advances. Unlike traditional feature selection methods, unsupervised feature selection (UFS) deals with unlabeled datasets, which are cheap and easy to obtain. Therefore, a large number of researchers have devoted themselves to developing UFS methods and have

This work was supported in part by the National Natural Science Foundation of China under Grant 12371306 and 12401430, the Innovation Program of Shanghai Municipal Education Commission under Grant 2023ZKZD47, and the Postdoctoral Fellowship Program of CPSF under Grant GZB20240801. (Corresponding author: Pan Shang.)

Xianchao Xiu and Chenyi Huang are with the School of Mechatronic Engineering and Automation, Shanghai University, Shanghai 200444, China (e-mail: xcxiu@shu.edu.cn; huangchenyi@shu.edu.cn).

Pan Shang is with the Academy of Mathematics and Systems Science, Chinese Academy of Sciences, Beijing 100190, China (e-mail: pshang@amss.ac.cn).

Wanquan Liu is with the School of Intelligent Systems Engineering, Sun Yat-sen University, Guangzhou 510275, China (e-mail: li-uwq63@mail.sysu.edu.cn).

shown promising performances in image processing [3]–[5], gene analysis [6]–[8], machine learning [9]–[11], and deep learning [12]–[14].

According to [2], existing UFS methods can be roughly divided into three categories based on different search strategies, including filtering methods, wrapper methods, and embedded methods. There are many representative UFS methods, such as Laplacian score (LapScore) [15], multi-cluster feature selection (MCFS) [16], unsupervised discriminative feature selection (UDFS) [17], structured optimal graph feature selection (SOGFS) [18], and robust neighborhood embedding (RNE) [19]. It is worth noting that the embedded methods combine the advantages of filtering and wrapping methods by directly integrating feature selection into the learning procedure [20].

As one of the most straightforward and accessible embedded methods, principal component analysis (PCA) stands out from UFS methods [21]. Despite of its excellent performance, one of the main drawbacks is the lack of feature interpretability [22]. To overcome this limitation, Yang et al. [17] proposed a sparse PCA model (UDFS), which incorporates an $\ell_{2,1}$ norm regularization term into PCA to promote sparsity of principal components. This approach was demonstrated to enhance the interpretability of features via selecting a subset of variables. Building upon the foundations laid by UDFS, Li et al. [23] combined PCA with an $\ell_{2,p}$ -norm with $p \in (0,1)$ regularization term, which is a non-convex version of sparse PCA. This novel sparse PCA variant, referred to as SPCAFS, aims to achieve feature sparsity and still retain the principal information simultaneously. Furthermore, Nie et al. [24] considered feature-sparsity constrained PCA (FSPCA), which is accomplished by enforcing $\ell_{2,0}$ -norm. Note that $\ell_{2,0}$ -norm is a direct choice to characterize the feature sparsity [25], meaning that FSPCA enables selecting a subset of features that are most representative and intrinsic. Note that $\ell_{2,1}$ -norm, $\ell_{2,p}$ -norm with $p \in (0,1)$, and $\ell_{2,0}$ -norm can be applied to characterize row sparsity, these sparse regularization terms attribute interpretability and robustness to PCA models, which are particularly beneficial for understanding the global data structures [26], [27].

However, when there exist locally intrinsic structures, a single sparse regularization term (e.g., $\ell_{2,1}$ -norm) may not be sufficient. Therefore, a bi-sparse optimization model with $\ell_{2,1}$ -norm and ℓ_{1} -norm regularization terms was proposed in [28], where $\ell_{2,1}$ -norm is used to characterize global structures and ℓ_{1} -norm is enforced to extract local intrinsic structures. For convenience, this group and sparse PCA model in [28] is denoted as GSPCA. In fact, the combination of $\ell_{2,1}$ -norm and ℓ_{1} -norm has been considered in multi-task feature selection and has shown excellent performance [29], [30]. We would also like to point out that although the idea of bi-sparse or double sparse has been applied in image denoising [31],

Methods **Objective Function Bi-sparse** Non-convex $\begin{aligned} & -\text{Tr}(W^{\top}SW) + \lambda \|W\|_{2,1} \\ & -\text{Tr}(W^{\top}SW) + \lambda \|W\|_{2,p}^{p}, \quad p \in (0,1) \end{aligned}$ **UDFS** [17] SPCAFS [23] Х $-\operatorname{Tr}(W^{\top}SW) + \lambda ||W||_{2.0}$ FSPCA [24] Х $\overline{-\text{Tr}(W^{\top}SW)} + \lambda_1 ||W||_{2,1} + \lambda_2 ||W||_1$ **GSPCA** [28] V $-\text{Tr}(W^{\top}SW) + \lambda_1 ||W||_{2,p}^p + \lambda_2 ||W||_q^q,$ **BSUFS**

TABLE I COMPARISONS OF PCA-BASED UFS METHODS.

compressed sensing [32], gene expression [33], and radar imaging [34], the involved double sparsity are constrained to different variables. In fact, $\ell_{2,p}$ -norm with $p \in [0,1)$ has good feature selection capabilities and ℓ_q -norm with $q \in [0,1)$ enables to capture the local structures. However, to our best knowledge, there is no work that constrains both of them to the same variable. A natural question is whether we can propose a bi-sparse non-convex PCA-based feature selection framework by inheriting the advantages of $\ell_{2,p}$ -norm with $p \in [0,1)$ and ℓ_q -norm with $q \in [0,1)$.

Motivated by the studies mentioned above, we propose a unified bi-sparse UFS method called BSUFS, which is a PCA model with $\ell_{2,p}$ -norm and ℓ_q -norm regularization terms, where p and q are within the range of [0,1). In fact, as shown in Table I, our proposed BSUFS is different from existing representative PCA-based UFS methods including UDFS [17], SPCAFS [23], FSPCA [24], and GSPCA [28]. It can be seen that our proposed BSUFS takes SPCAFS and FSPCA as special cases and has higher flexibility than convex relaxations, i.e., UDFS and GSPCA. Of course, the choice of p and q may be affected by the specific data structure, which will be discussed in Subsection IV-D, and it is confirmed that combining the values of 0 and (0,1) into [0,1) is of great significance. In addition, the idea of bi-sparse optimization is not limited to feature selection, but can be easily extended to other fields of image processing.

The main contributions of this paper can be summarized in the following three aspects:

- We develop a novel BSUFS method to learn both global and local structures simultaneously. The values of p and q are set in the range of [0,1), which offers a unified way to achieve bi-sparse feature selection.
- We design an efficient proximal alternating minimization (PAM) algorithm and prove that the generated sequence with any initial point converges to the critical point and satisfies the first-order optimality conditions.
- We conduct sufficient numerical experiments to evaluate the performance of BSUFS. In particular, we analyze the parameter effects of $p,q \in [0,1)$ and show that in feature selection, p plays a dominant role, while q serves as a complementary role, both of which are indispensable.

The structure of this paper is outlined as follows. Section III introduces notations and related works. Section III presents the proposed model, optimization algorithm, and convergence. Section IV shows the numerical results, ablation experiments, and discussions. Section V concludes this paper. The detailed proof is provided in the appendix.

II. PRELIMINARIES

This section introduces some notations and related preliminaries used throughout this paper.

A. Notations

In this paper, matrices are represented by capital letters, vectors by boldface letters, and scalars by lowercase letters. Let \mathbb{R}^d and $\mathbb{R}^{m \times n}$ be the sets of all d-dimensional vectors and $m \times n$ -dimensional matrices, respectively. For any vector $\mathbf{x} \in \mathbb{R}^d$, its i-th element is denoted as x_i . The ℓ_2 -norm of \mathbf{x} is $\|\mathbf{x}\| = (\sum_{i=1}^d x_i^2)^{1/2}$. For any matrix $X \in \mathbb{R}^{m \times n}$, x_{ij} represents its ij-th element, \mathbf{x}^i and \mathbf{x}_i represent its i-th row and i-th column, respectively. The Frobenius norm of X is $\|X\|_{\mathbf{F}} = (\sum_{i=1}^m \sum_{j=1}^n x_{ij}^2)^{1/2}$. For $p,q \in (0,1)$, the $\ell_{2,p}$ -norm of X is defined as $\|X\|_{2,p} = (\sum_{i=1}^m \|\mathbf{x}^i\|^p)^{1/p}$ and the ℓ_q -norm is $\|X\|_q = (\sum_{i=1}^m \sum_{j=1}^n |x_{ij}|^q)^{1/q}$. When p,q=1, they are exactly $\ell_{2,1}$ -norm and ℓ_1 -norm. In addition, $\|X\|_{2,0}$ and $\|X\|_0$ count the numbers of non-zero rows and non-zero elements of X, respectively. A further notation will be introduced wherever it appears.

B. PCA Basis

Consider a data matrix $X = (\mathbf{x}_1, \mathbf{x}_2, \dots, \mathbf{x}_n) \in \mathbb{R}^{d \times n}$ with $\mathbf{x}_i \in \mathbb{R}^d$. Denote W as a projection matrix and $W = (\mathbf{w}_1, \mathbf{w}_2, \dots, \mathbf{w}_m) \in \mathbb{R}^{d \times m}$, where $\mathbf{w}_i \in \mathbb{R}^d$, $\|\mathbf{w}_i\| = 1$ and $\mathbf{w}_i^{\top} \mathbf{w}_i = 0$ for $i \neq j$. Here, it is supposed that m < n.

Mathematically, PCA can be represented in a trace formulation with an orthogonal constraint as

$$\begin{aligned} \min_{W \in \mathbb{R}^{d \times m}} & -\operatorname{Tr}\left(W^{\top}XX^{\top}W\right) \\ \text{s.t.} & W^{\top}W = I_m, \end{aligned} \tag{1}$$

where the data is assumed to be centralized. For the general case that the data is not centralized, PCA can be written as

$$\min_{W \in \mathbb{R}^{d \times m}} - \operatorname{Tr} \left(W^{\top} S W \right)$$
s.t.
$$W^{\top} W = I_m,$$
(2)

where $S = XHX^{\top}$ and $H = I_n - \frac{1}{n}\mathbf{1}\mathbf{1}^{\top}$ with $\mathbf{1} \in \mathbb{R}^n$ being a vector whose elements are all 1.

Without loss of generality, denote $\mathbf{w}^{i\top}$ as the transpose of \mathbf{w}^i , where \mathbf{w}^i is the *i*-th row of W. In feature selection, it can be found that $\mathbf{w}^{i\top}$ represents the transformation vector associated with the *i*-th feature in W as

$$\mathbf{z}_{i} = (\mathbf{w}^{1\top}, \ \mathbf{w}^{2\top}, \ \dots, \mathbf{w}^{d\top}) \begin{pmatrix} x_{1} \\ x_{2} \\ \vdots \\ x_{d} \end{pmatrix}. \tag{3}$$

Accordingly, $\|\mathbf{w}^i\|$ can be used to measure the importance of the i-th feature [35].

C. Sparse PCA

Yang et al. [17] proposed a sparse PCA model called UDFS, which is given by

$$\min_{W \in \mathbb{R}^{d \times m}} - \text{Tr}(W^{\top}SW) + \lambda \|W\|_{2,1}$$
s.t.
$$W^{\top}W = I_{m}.$$
(4)

where $\lambda \geq 0$ is the regularization parameter. By introducing $\ell_{2,1}$ -norm into the objective function of (2), UDFS can obtain a row-sparse projection matrix W, thereby improving the performance of feature selection.

In recent years, non-convex optimization has been rapidly developed, which can provide more possibilities than convex optimization [36]-[38]. With this advantage, Li et al. [23] proposed SPCAFS as

$$\min_{W \in \mathbb{R}^{d \times m}} - \text{Tr}(W^{\top}SW) + \lambda \|W\|_{2,p}^{p}$$
s.t. $W^{\top}W = I_{m}$, (5)

where $p \in (0,1)$, and demonstrated that when p = 1/2, its performance is better than the convex relaxation in (4). Actually, when p = 1, it degenerates to (4).

Different from these single structured sparse approaches, Zhu et al. [28] further integrated ℓ_1 -norm to objective of (4), which is denoted as GSPCA and given by

$$\min_{W \in \mathbb{R}^{d \times m}} -\text{Tr}(W^{\top}SW) + \lambda_1 \|W\|_{2,1} + \lambda_2 \|W\|_1$$
s.t. $W^{\top}W = I_m$. (6)

It is numerically verified that GSPCA can better select representative features in both global and local senses due to the introduction of $\ell_{2,1}$ -norm and ℓ_1 -norm regularization terms.

III. THE PROPOSED METHOD

This section first presents our proposed bi-sparse and nonconvex UFS model, and then shows an optimization algorithm with rigorous convergence analysis.

A. Model Construction

In order to inherit the advantages of non-convex optimization and bi-sparse optimization, we propose a sparse PCA variant called BSUFS, which is formulated as

$$\min_{W \in \mathbb{R}^{d \times m}} -\text{Tr}(W^{\top}SW) + \lambda_1 \|W\|_{2,p}^p + \lambda_2 \|W\|_q^q$$
s.t.
$$W^{\top}W = I_m,$$
(7)

where $p,q \in [0,1)$ and $\lambda_1,\lambda_2 \geq 0$ are the parameters to control the bi-sparse regularization terms.

Compared with the existing PCA-based UFS methods listed in Table I, the following conclusions can be made:

- When $\lambda_2 = 0$ in (7), our proposed BSUFS unifies FSPCA and SPCAFS.
- When p and q tend to 1 in (7), our proposed BSUFS reduces to GSPCA and covers UDFS.

Algorithm 1 Optimization algorithm for BSUFS

Input: Data $X \in \mathbb{R}^{d \times n}$, parameters $p, q, \lambda_1, \lambda_2, \beta_1, \beta_2, \tau_1, \tau_2, \tau_3$, calculate $H = I_n - \frac{1}{n} \mathbf{1} \mathbf{1}^\top, S = X H X^\top$

Initialize: $k = 0, W^k, U^k, V^k$

While not converged do

- 1: Update W^{k+1} by (11)
- 2: Update U^{k+1} by (12)
- 3: Update V^{k+1} by (13)
- 4: Check convergence: If $\frac{|f^{k+1}-f^k|}{\max\{|f^k|,1\}}<10^{-4}$ or k>500, then stop. Otherwise, k=k+1

End While

• Besides the Riemannian manifold constraint $W^{\top}W =$ I_m , the introduced $\ell_{2,p}$ -norm and ℓ_q -norm in (7) makes our proposed BSUFS non-convex.

In summary, BSUFS can provide flexible sparse solutions by choosing different p and q in the range of [0,1), thus facilitating feature selection.

B. Optimization Algorithm

The non-convex property of (7) makes it difficult to develop a computational algorithm. Here, we provide an efficient and convergent optimization scheme.

By utilizing auxiliary variables W = V, W = U, (7) can be reformulated as

$$\min_{W,U,V \in \mathbb{R}^{d \times m}} - \text{Tr}(W^{\top}SW) + \lambda_1 \|V\|_{2,p}^p + \lambda_2 \|U\|_q^q$$
s.t. $W^{\top}W = I_m, \ W = V, \ W = U.$ (8)

Then, introduce the indicator function

$$\Phi(W) = \begin{cases} 0, & W^{\top}W = I_m \\ +\infty, & \text{otherwise,} \end{cases}$$
 (9)

and rewrite (8) as the following equivalent form

$$\min_{W,U,V \in \mathbb{R}^{d \times m}} - \text{Tr}(W^{\top}SW) + \lambda_1 \|V\|_{2,p}^p + \lambda_2 \|U\|_q^q + \frac{\beta_1}{2} \|W - U\|_F^2 + \frac{\beta_2}{2} \|W - V\|_F^2 + \Phi(W), \tag{10}$$

where $\beta_1, \beta_2 > 0$ are the penalty parameters. Denote the objective function of (10) as f(W, U, V). Under the PAM framework, each variable can be updated alternately via

$$W^{k+1} = \underset{W \in \mathbb{R}^{d \times m}}{\min} f(W, U^k, V^k) + \frac{\tau_1}{2} \|W - W^k\|_{F}^2, \quad (11)$$

$$U^{k+1} = \underset{U \in \mathbb{R}^{d \times m}}{\arg \min} f(W^{k+1}, U, V^k) + \frac{\tau_2}{2} ||U - U^k||_F^2, \quad (12)$$

$$V^{k+1} = \underset{V \in \mathbb{R}^{d \times m}}{\operatorname{arg\,min}} \ f(W^{k+1}, U^{k+1}, V) + \frac{\tau_3}{2} \|V - V^k\|_{\mathcal{F}}^2, \ (13)$$

where $\tau_1, \tau_2, \tau_3 > 0$ and k is the iteration number. The overall scheme is presented in Algorithm 1, and the update rules for W, U, and V are analyzed below.

Algorithm 2 Solution of (11)

Input: Data $S \in \mathbb{R}^{d \times d}$, $U^k \in \mathbb{R}^{d \times m}$, $V^k \in \mathbb{R}^{d \times m}$, parameters $\beta_1, \, \beta_2, \, \tau_1, \, \varepsilon, \, \Delta' > 0, \, \rho' \in [0, \frac{1}{4})$

Output: W^k

Initialize: $i = 0, W_i^k \in St(d, m), \Delta_i \in (0, \Delta')$

While not converged do

1: Obtain η_i by solving (21) with $W=W_i^k$ and $\Delta=\Delta_i$

2: Compute ρ_i from (22) with $W = W_i^k$

3: **if** $\rho_i < \frac{1}{4}$ **then**

4: $\Delta_{i+1} = \frac{1}{4}\Delta_i$ 5: **else if** $\rho_i > \frac{3}{4}$ and $\|\eta_i\| = \Delta_i$ **then**

 $\Delta_{i+1} = \min(2\Delta_i, \Delta')$

7: else

 $\Delta_{i+1} = \Delta_i$ 8:

9: end if

10: if $\rho_i > \rho'$ then

 $W_{i+1}^k = R_W(\eta_i)$

12: **else**

13: $W_{i+1}^k = W_i^k$ 14: **end if**

15: Check convergence: If grad $g(W_{i+1}^k) < 10^{-6}$ or i > 100, then stop. Otherwise, i = i + 1

End While

1) Update W by fixing U and V: (11) can be expressed as

$$\min_{W^{\top}W=I_{m}} g(W) = -\text{Tr}(W^{\top}SW) + \frac{\beta_{1}}{2} \|W - U^{k}\|_{F}^{2} + \frac{\beta_{2}}{2} \|W - V^{k}\|_{F}^{2} + \frac{\tau_{1}}{2} \|W - W^{k}\|_{F}^{2}.$$
(14)

The Euclidean gradient of q(W) is

$$\nabla g(W) = -2SW + \beta_1(W - U^k) + \beta_2(W - V^k) + \tau_1(W - W^k),$$
(15)

and the Euclidean Hessian is

$$\nabla^2 q(W) = -2I_m \otimes S + (\beta_1 + \beta_2 + \tau_1)I_{dm}, \tag{16}$$

where \otimes represents the Kronecker product.

Let $\operatorname{St}(d,m) = \{W \in \mathbb{R}^{d \times m} \mid W^\top W = I_m\}$. Then, (14) is a Riemannian manifold optimization problem and can be reformulated as

$$\min_{W \in St(d,m)} g(W). \tag{17}$$

To implement the trust region algorithm [39], there are two basic elements, i.e., the search direction and the trust-region ratio. The search direction relies on the Riemannian gradient and Riemannian Hessian of the objective function g(W) in (17). Specifically, the Riemannian gradient can be obtained by projecting its Euclidean gradient onto the tangent space of the Riemannian manifold, i.e.,

$$\operatorname{grad} g(W) = \mathcal{P}_{W}(\nabla g(W))$$

$$= \nabla g(W) - W \operatorname{sym}(W^{\top} \nabla g(W)), \tag{18}$$

where $\mathcal{P}_W(\nabla g(W))$ is the projection of the Euclidean gradient onto the tangent space of the Riemannian manifold, and $\operatorname{sym}(X) = (X + X^{\top})/2$ extracts the symmetric part of a square matrix X. The Riemannian Hessian can be obtained by projecting its Euclidean Hessian onto the tangent space of the Riemannian manifold, i.e.,

$$\operatorname{Hess} g(W) = \mathcal{P}_W(\nabla^2 g(W))$$

= $\nabla^2 g(W) - W \operatorname{sym}(W^{\top} \nabla^2 g(W)),$ (19)

which can be approximated by

$$\operatorname{Hess} g(W) \approx \frac{\operatorname{grad} g(W + \varepsilon I) - \operatorname{grad} g(W)}{\varepsilon}, \qquad (20)$$

where ε is a small positive constant.

Then, the search direction of the trust region algorithm is derived by solving the following problem

$$\min_{\eta \in \mathcal{T}_{\mathcal{W}} \operatorname{St}(d,m)} m_{W}(\eta) = g(W) + \operatorname{Tr}(\eta^{\top} \operatorname{grad} g(W))
+ \frac{1}{2} \operatorname{vec}(\eta)^{\top} \operatorname{Hess} g(W) \operatorname{vec}(\eta)
\text{s.t.} \operatorname{Tr}(\eta^{\top} W \eta^{\top}) \leq \Delta^{2},$$
(21)

where $vec(\eta)$ denotes the vector obtained by stacking its columns into a single vector, Δ is the trust-region radius, and $T_W \operatorname{St}(d, m)$ is the tangent space of the manifold at W.

Finally, the trust region ratio is determined by

$$\rho = \frac{g(W) - g(R_W(\eta))}{m_W(0) - m_W(\eta)},\tag{22}$$

where $R_W(\eta)$ is the retraction of η onto the Riemannian manifold.

Therefore, the trust-region Riemannian manifold optimization algorithm of solving (11) is given in Algorithm 2.

2) Update U by fixing W and V: After updating W, (12)can be solved by

$$\min_{U \in \mathbb{R}^{d \times m}} \lambda_2 \|U\|_q^q + \frac{\beta_1}{2} \|W^{k+1} - U\|_F^2 + \frac{\tau_2}{2} \|U - U^k\|_F^2. \tag{23}$$

By expanding the norm terms in (23), this subproblem can be rewritten as the form of

$$\min_{U \in \mathbb{R}^{d \times m}} \ \lambda_2 \|U\|_q^q + \frac{\beta_1 + \tau_2}{2} \|U - Y\|_F^2, \tag{24}$$

where

$$Y = \frac{\beta_1}{\beta_1 + \tau_2} W^{k+1} + \frac{\tau_2}{\beta_1 + \tau_2} U^k.$$

By considering each element of the matrix separately, the optimization problem can be reformulated as

$$\min_{u_{ij} \in \mathbb{R}} \lambda_2 |u_{ij}|^q + \frac{\beta_1 + \tau_2}{2} (u_{ij} - y_{ij})^2.$$
 (25)

The solution to this problem is the proximal operator of the $|\cdot|^q$, whose result is reviewed in the following lemma.

Lemma 3.1: Consider the proximal operator

$$\operatorname{Prox}(a,\lambda) = \underset{x}{\operatorname{argmin}} \lambda |x|^{q} + \frac{1}{2}(x-a)^{2}$$

$$= \begin{cases} \{0\}, & |a| < \kappa(\lambda,q), \\ \{0,\operatorname{sgn}(a)c(\lambda,q)\}, & |a| = \kappa(\lambda,q), \\ \{\operatorname{sgn}(a)\varpi_{q}(|a|)\}, & |a| > \kappa(\lambda,q), \end{cases}$$
(26)

where

$$c(\lambda, p) = (2\lambda(1-q))^{\frac{1}{2-q}} > 0,$$

$$\kappa(\lambda, q) = (2-q)\lambda^{\frac{1}{2-q}} (2(1-q))^{\frac{q+1}{q-2}},$$

$$\varpi_q(a) \in \{x \mid x-a+\lambda q \operatorname{sgn}(x) x^{q-1} = 0, x > 0\}.$$
(27)

More details can be found in [40].

According to Lemma 3.1, the solution of (25) can be easily obtained by

$$u_{ij} = \text{Prox}\left(y_{ij}, \frac{\lambda_2}{\beta_1 + \tau_2}\right).$$
 (28)

3) Update V by fixing W and U: Once W and U have been updated, (13) can be calculated via

$$\min_{V \in \mathbb{R}^{d \times m}} \lambda_1 \|V\|_{2,p}^p + \frac{\beta_2}{2} \|W^{k+1} - V\|_{\mathcal{F}}^2 + \frac{\tau_3}{2} \|V - V^k\|_{\mathcal{F}}^2. \tag{29}$$

It is easy to reformulate (29) as

$$\min_{V \in \mathbb{R}^{d \times m}} \ \lambda_1 \|V\|_{2,p}^p + \frac{\beta_2 + \tau_3}{2} \|V - Z\|_{\mathsf{F}}^2, \tag{30}$$

where

$$Z = \frac{\beta_2}{\beta_2 + \tau_3} W^{k+1} + \frac{\tau_3}{\beta_2 + \tau_3} V^k.$$

It can be further decomposed into a series of vector optimization problems as

$$\min_{\mathbf{v}^{i} \in \mathbb{R}^{m}} \lambda_{1} \|\mathbf{v}^{i}\|^{p} + \frac{\beta_{2} + \tau_{3}}{2} \|\mathbf{v}^{i} - \mathbf{z}^{i}\|^{2}, \tag{31}$$

where $i \in \{1, 2, \dots, d\}$. Following a similar idea as stated in Lemma 3.1, this subproblem can be solved by

$$\mathbf{v}^{i} = \operatorname{Prox}\left(\|\mathbf{z}^{i}\|, \frac{\lambda_{1}}{\beta_{2} + \tau_{3}}\right) \cdot \frac{\mathbf{z}^{i}}{\|\mathbf{z}^{i}\|}.$$
 (32)

Remark 3.2: For Algorithm 1, it is suggested to update U^{k+1} first for eliminating the interference caused by noise and then update V^{k+1} for selecting discriminative features.

C. Convergence Analysis

Due to the non-convex nature of f(W,U,V) and the Riemannian manifold constraint, it is relatively difficult to give convergence results. Fortunately, with the help of the Kurdyka-Lojasiewicz (K-L) property [41], [42], we establish the global convergence of Algorithm 1 and provide a detailed proof in the appendix.

Theorem 3.3: Assume $\{(W^k, U^k, V^k)\}_{k \in \mathbb{N}}$ is generated by Algorithm 1. Then, the sequence $\{(W^k, U^k, V^k)\}_{k \in \mathbb{N}}$ globally converges to a critical point of f(W, U, V), i.e.,

$$0 \in \partial f(W^*, U^*, V^*) \tag{33}$$

with $\lim_{k\to +\infty}(W^k,U^k,V^k)=(W^*,U^*,V^*)$ and $\partial f(\cdot)$ being the limiting subdifferential set.

Remark 3.4: In fact, this theorem implies that, by initializing Algorithm 1 with an arbitrary random point (W^0, U^0, V^0) , the generated sequence converges to a point that satisfies the first-order optimality condition of f(W, U, V).

TABLE II INFORMATION OF SELECTED DATASETS.

| Туре | Datasets | Features | Samples | Classes | |
|---------------------|------------|----------|---------|---------|--|
| Synthetic datasets | Dartboard1 | 9 | 1000 | 4 | |
| Synthetic datasets | Diamond9 | 9 | 3000 | 9 | |
| | COIL20 | 1024 | 1440 | 20 | |
| | USPS | 256 | 1000 | 10 | |
| | LUNG | 325 | 73 | 7 | |
| Real-world datasets | GLIOMA | 4434 | 50 | 4 | |
| Real-world datasets | UMIST | 644 | 575 | 20 | |
| | pie | 1024 | 1166 | 53 | |
| | Isolet | 617 | 1560 | 26 | |
| | MSTAR | 1024 | 2425 | 10 | |

IV. NUMERICAL STUDIES

To illustrate the effectiveness of the proposed BSUFS, this section presents extensive comparisons with several benchmark UFS methods, including LapScore [15], MCFS [16], SOGFS [18], RNE [19], UDFS [17], SPCAFS [23], FSPCA [24], and GSPCA [28].

Subsection IV-A describes datasets, parameter settings, and evaluation metrics. Subsection IV-B presents numerical experiments on synthetic and real-world datasets. Subsection IV-C provides ablation experiments. Subsection IV-D analyzes the effects of *p* and *q*. Subsection IV-E gives more discussions.

A. Experimental Setup

1) Dataset Description: There are two synthetic datasets and eight real-world datasets that are used to validate the performance of our proposed BSUFS. For more details about these datasets, please refer to Table II.

The two synthetic datasets¹ are generated by assigning specific distributions to the first two features, while the remaining seven features are filled with Gaussian noise. The eight real-world datasets encompass a diverse range of domains, such as Isolet² for spoken letter recognition, MSTAR_SOC_CNN³ (referred to as MSTAR) for deep learning, GLIOMA² and lung_discrete² (referred to as LUNG) for biological information, COIL20², USPS², pie⁴, and umist⁵ for image processing.

2) Compared Methods and Parameter Settings: In the experiments, LapScore, MCFS, SOGFS, RNE, and UDFS are directly implemented by the AutoUFSTool toolbox⁶. SPCAFS⁷ and FSPCA⁸ are both from the authors' GitHub repositories. In addition, GSPCA is coded by ourselves based on the algorithm framework provided in their paper.

For LapScore, MCFS, SOGFS, and RNE, the value of *k*-neighbors is set as 5. For SOGFS, SPCAFS, GSPCA, and BSUFS, their regularization parameters are selected from

¹https://github.com/milaan9/Clustering-Datasets

 $^{^2} https://jundongl.github.io/scikit-feature/datasets.html\\$

³https://github.com/zjj20212035/SPCA-PSD

⁴https://data.nvision2.eecs.yorku.ca/PIE_dataset/

⁵https://github.com/saining/PPSL/blob/master/Platform/Data/UMIST/UMIST.mat

⁶https://github.com/farhadabedinzadeh/AutoUFSTool

⁷https://github.com/quiter2005/algorithm

⁸https://github.com/tianlai09/FSPCA

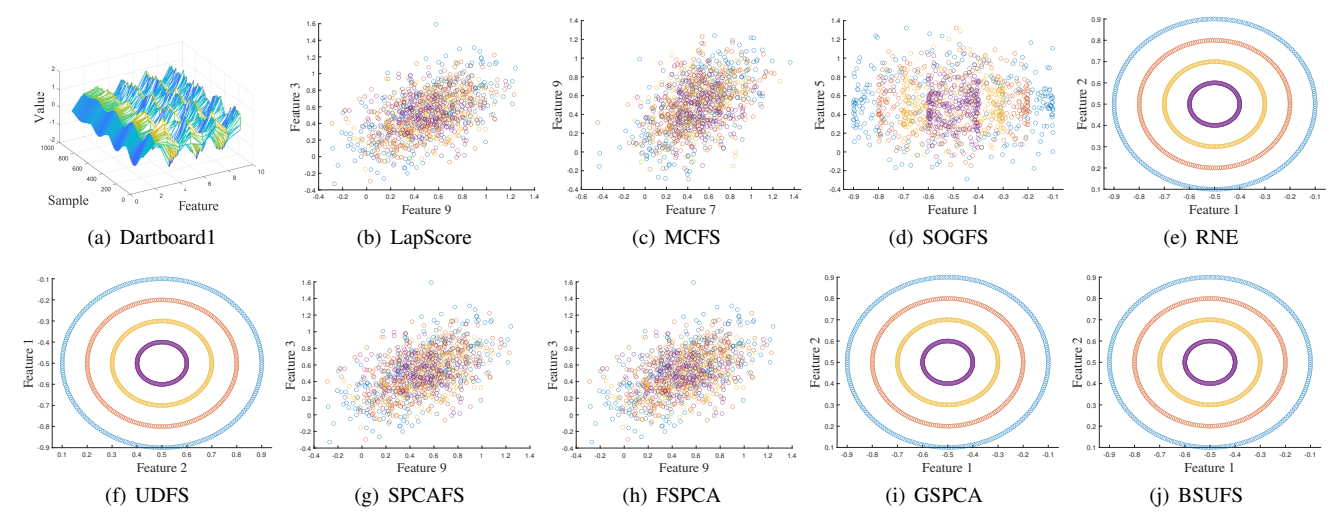


Fig. 1. Visual comparisons on the Dartboard1 dataset, where (a) is the dataset distribution, and (b)-(j) are the feature selection results.

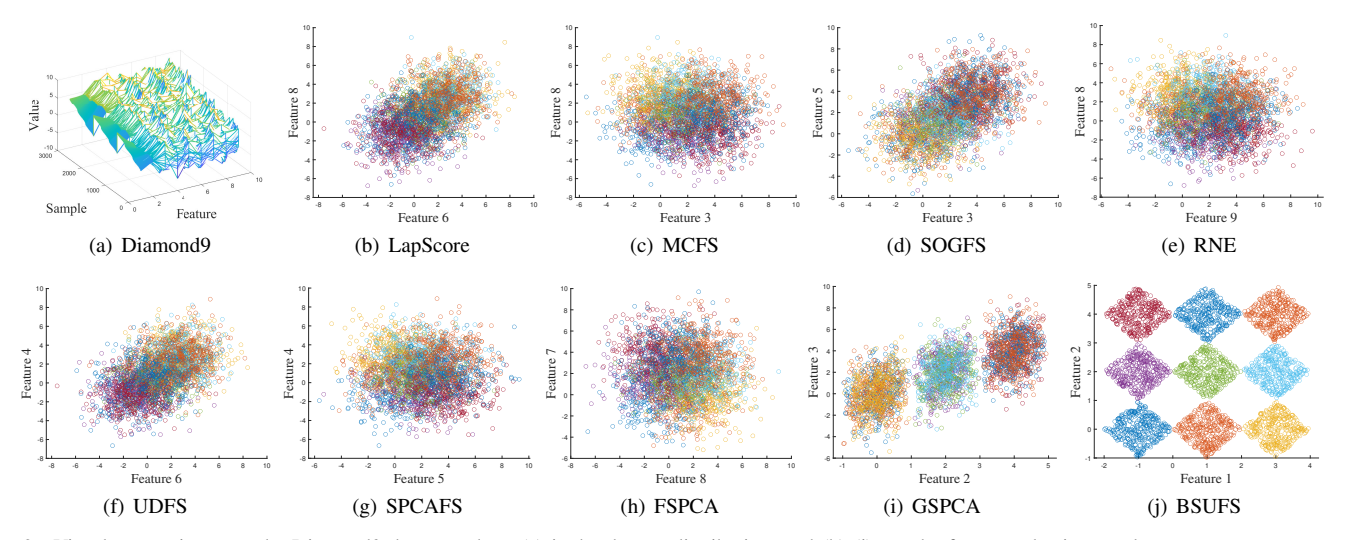


Fig. 2. Visual comparisons on the Diamond9 dataset, where (a) is the dataset distribution, and (b)-(j) are the feature selection results.

the candidate set $\{10^{-6}, 10^{-4}, 10^{-2}, 10^{0}, 10^{2}, 10^{4}, 10^{6}\}$. As suggested in [40], [43], the values of p and q for BSUFS are selected from $\{0, 1/2, 2/3\}$. For other parameters, the default values or the best parameters provided by the authors are used.

3) Evaluation Metrics: Two key metrics are applied to evaluate these compared methods, including clustering accuracy (ACC) and normalized mutual information (NMI). Following a similar way in [23], we select the number of features across all datasets in increments of 10, ranging from 10 to 100. To be fair and counteract the variability introduced by different initial conditions, 50 repetitions of the k-means clustering algorithm are conducted. This means that the final results are reported as the mean and standard deviation of the 50 repetitions.

B. Numerical Experiments

1) Synthetic Results: In this experiment, various UFS methods are conducted on two synthetic datasets. Each UFS method is applied to obtain scores for all nine features and the top two features are selected. After that, the selected features

are visualized in scatter diagrams alongside the samples. The feature selection results are shown in Fig. 1 and Fig. 2.

It can be concluded that our proposed BSUFS consistently selects discriminative features, while the other methods fail to select the correct features in some cases. For the Dartboard1 dataset in Fig. 1, RNE, UDFS, GSPCA, and BSUFS are all capable of identifying the appropriate features, comparing to the other methods. The feature selection results for the Diamond9 dataset demonstrate that BSUFS is the only method that can successfully identify the two most discriminative features. All those results suggest the effectiveness of our proposed BSUFS on the synthetic datasets.

2) Real-world Results: This section presents numerical results on real-world datasets. Here is another compared method called ALLfea, which stands for all features used for clustering and is the gold standard for comparison. Fig. 3 and Fig. 4 show the average values of ACC and NMI for 50 repetitions under different selected feature numbers. Table III and Table IV summarize the detailed results, with the top two performers marked in red and blue except for ALLfea. To be specific, we

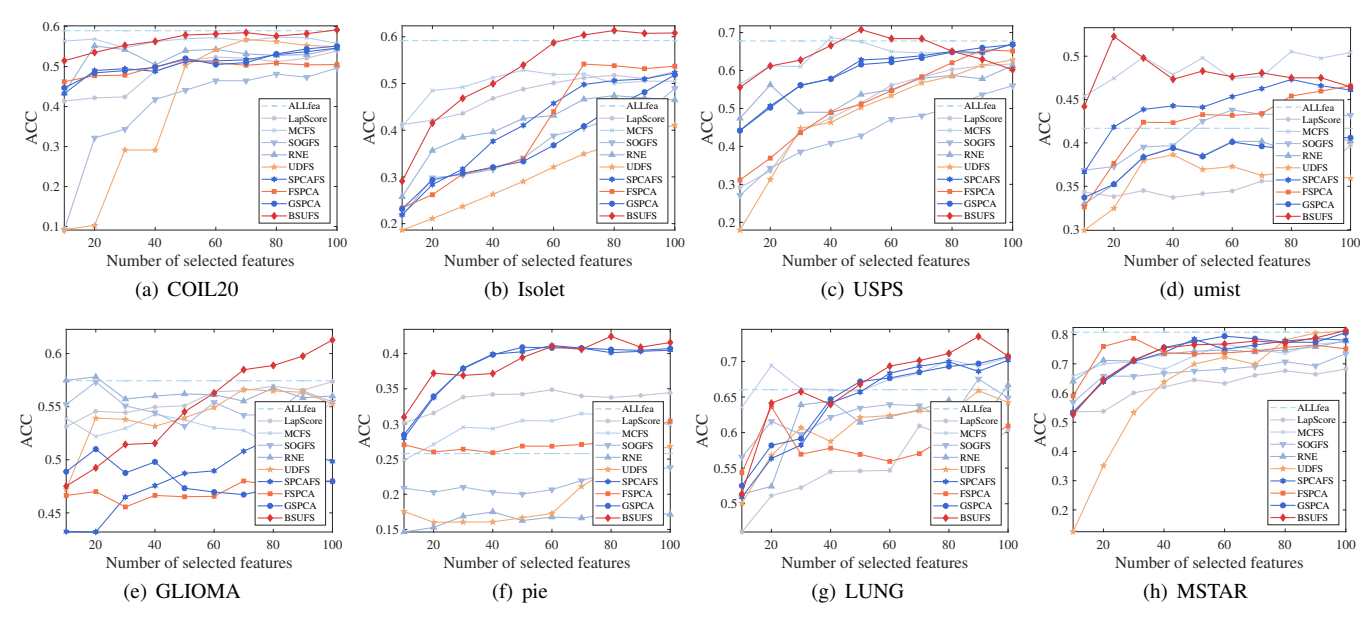


Fig. 3. Visual comparisons of the ACC metric under different datasets with different number of selected features.

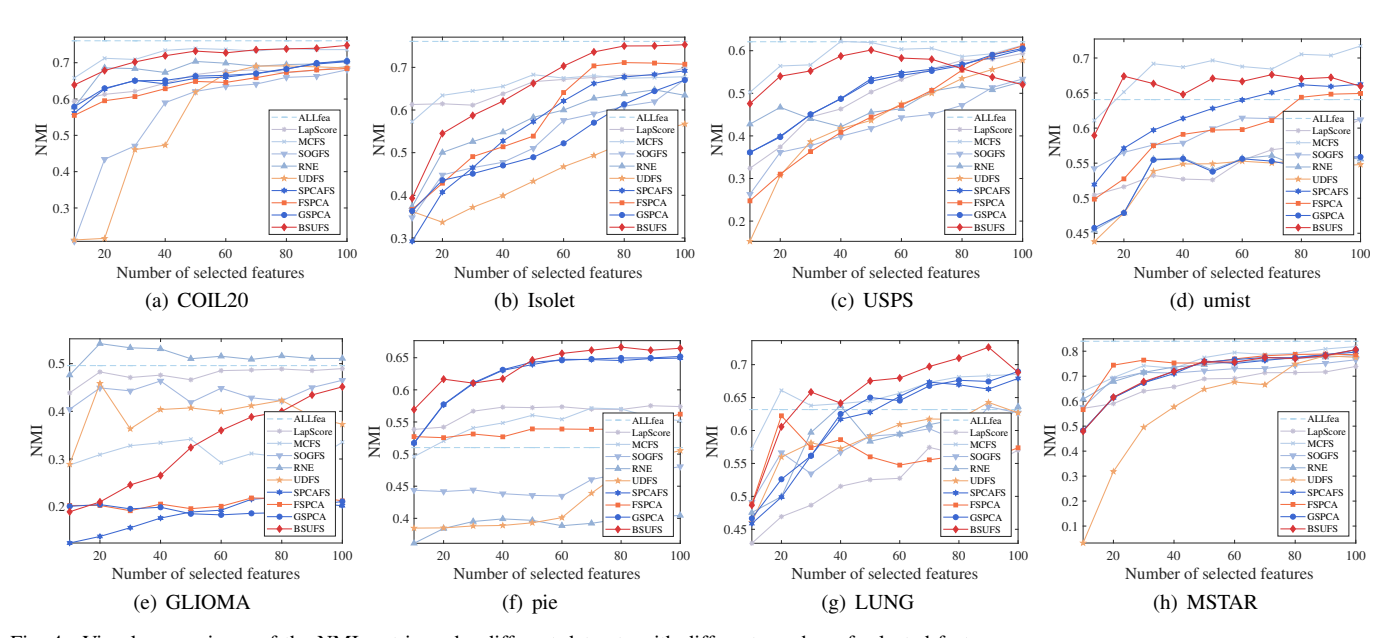


Fig. 4. Visual comparisons of the NMI metric under different datasets with different number of selected features.

set the number of selected features for each method from 10 to 100 and report the best feature selection performance with the number of features shown in bracket.

For the ACC metric, our proposed BSUFS generally outperforms other methods across all datasets with higher ACCs. In Fig. 3, almost all BSUFS lines are higher than other lines under different number of selected features, which implies that BSUFS performs better than others in terms of ACC. In Table III, all results for BSUFS are colored as red because the average ACC values under this method are the largest on these real-world datasets. Actually, our proposed BSUFS outperforms ALLfea on some datasets. For example, on the GLIOMA dataset, BSUFS attains an accuracy of 61.28%, which is superior to the 57.44% for ALLfea. In particular, from Table III, it can be seen that BSUFS achieves at least

an average improvement of 5.57% than GSPCA, 7.95% than FSPCA, and 5.88% than SPCAFS, which validates the efficacy of our proposed BSUFS.

For the corresponding NMI metric, our proposed BSUFS also exhibits better performance than other compared methods. Although not all BSUFS lines in Fig. 4 are higher than others, they are still the most lines. As shown in Table IV, BSUFS achieves significantly higher NMI scores than other competitors as well as ALLfea on the pie and LUNG datasets. On average, our proposed BSUFS improves NMI values by at least 3.14% compared to other methods except for ALLfea.

Overall, BSUFS outperforms compared methods on many real-world datasets by achieving higher ACC and NMI values. These superior performances highlight its potential as a valuable tool for UFS. On the other hand, achieving higher

TABLE III

AVERAGE ACC (MEAN $\%\pm$ STD %) AND NUMBER OF SELECTED FEATURES (IN BRACKET) OF K-MEANS CLUSTERING. THE TOP TWO VALUES ARE MARKED AS RED AND BLUE.

| Datasets | ALLfea | LapScore | MCFS | SOGFS | RNE | UDFS | SPCAFS | FSPCA | GSPCA | BSUFS |
|----------|------------------|------------|------------|------------|------------------|------------|------------|------------|------------|------------|
| COIL20 | 58.97±4.99 | 53.91±3.61 | 57.35±3.83 | 49.66±3.63 | 55.16±3.35 | 56.77±3.09 | 54.63±3.64 | 51.71±3.05 | 55.12±2.67 | 59.18±3.49 |
| COIL20 | (10) | (100) | (80) | (100) | (20) | (70) | (100) | (50) | (100) | (100) |
| Isolet | 59.18±3.19 | 52.55±2.83 | 52.87±2.87 | 48.93±2.69 | 47.39±2.91 | 41.11±1.71 | 52.26±2.81 | 54.15±2.69 | 51.84±2.82 | 61.34±3.33 |
| Isolet | (10) | (100) | (50) | (100) | (80) | (100) | (100) | (70) | (100) | (80) |
| USPS | 67.79 ± 4.96 | 61.76±4.52 | 68.70±4.10 | 56.00±3.48 | 61.28 ± 3.46 | 62.83±3.79 | 66.98±3.92 | 65.43±4.90 | 66.79±4.10 | 70.77±3.73 |
| CSIS | (10) | (100) | (40) | (100) | (100) | (100) | (100) | (90) | (100) | (50) |
| umist | 41.68 ± 2.46 | 39.71±3.28 | 50.54±4.16 | 43.81±2.98 | 41.01±2.25 | 38.64±1.61 | 47.32±3.48 | 46.58±2.34 | 40.65±2.29 | 52.29±3.61 |
| umst | (10) | (100) | (80) | (60) | (90) | (40) | (80) | (100) | (90) | (20) |
| GLIOMA | 57.44 ± 6.40 | 57.36±3.60 | 55.52±9.25 | 57.32±6.47 | 57.80±2.98 | 56.64±6.47 | 52.08±3.64 | 48.04±5.26 | 51.00±5.08 | 61.28±9.01 |
| GLIOMA | (10) | (100) | (100) | (20) | (20) | (70) | (80) | (90) | (20) | (100) |
| pie | 25.79 ± 1.39 | 34.86±1.43 | 31.46±1.47 | 23.78±1.19 | 17.49 ± 0.76 | 26.82±1.32 | 41.16±2.46 | 30.39±1.43 | 40.90±1.85 | 42.45±1.74 |
| pic | (10) | (60) | (70) | (100) | (40) | (100) | (60) | (100) | (50) | (80) |
| LUNG | 66.03 ± 7.23 | 60.93±8.02 | 70.55±7.66 | 67.53±7.73 | 66.68 ± 8.32 | 65.89±7.43 | 70.16±7.71 | 63.62±5.45 | 70.68±7.41 | 73.51±6.80 |
| Lerve | (10) | (70) | (100) | (90) | (100) | (90) | (100) | (20) | (100) | (90) |
| MSTAR | 80.81±8.76 | 68.21±4.57 | 77.60±8.32 | 73.46±5.61 | 77.82±6.16 | 81.25±7.48 | 78.63±8.68 | 78.74±5.20 | 80.65±6.47 | 81.43±6.89 |
| MISTAK | (10) | (100) | (100) | (100) | (100) | (100) | (90) | (30) | (100) | (100) |
| Average | 57.21±4.92 | 53.66±3.98 | 58.07±5.21 | 52.56±4.22 | 53.08±3.77 | 53.74±4.11 | 57.90±4.54 | 54.83±3.79 | 57.21±4.09 | 62.78±4.83 |

TABLE IV AVERAGE NMI (MEAN $\%\pm$ STD %) AND NUMBER OF SELECTED FEATURES (IN BRACKET) OF K-MEANS CLUSTERING. THE TOP TWO VALUES ARE MARKED AS RED AND BLUE.

| Datasets | ALLfea | LapScore | MCFS | SOGFS | RNE | UDFS | SPCAFS | FSPCA | GSPCA | BSUFS |
|----------|------------------|------------|------------|------------|------------------|------------|------------|------------|------------|-------------|
| COIL20 | 76.04±1.69 | 69.01±1.53 | 73.98±1.79 | 68.03±1.59 | 70.76±2.07 | 69.12±1.17 | 70.29±1.31 | 68.41±1.60 | 70.44±1.37 | 74.78±1.79 |
| COIL20 | (10) | (100) | (80) | (100) | (100) | (80) | (100) | (100) | (100) | (100) |
| Isolet | 76.09 ± 1.77 | 69.86±1.26 | 68.29±1.05 | 67.15±1.45 | 64.74 ± 1.28 | 56.73±1.05 | 69.18±1.33 | 71.12±1.11 | 67.02±1.43 | 75.32±1.22 |
| Isolct | (10) | (100) | (50) | (90) | (100) | (100) | (100) | (80) | (100) | (100) |
| USPS | 62.11±2.24 | 59.37±1.98 | 62.18±2.01 | 53.36±1.83 | 52.77±2.01 | 57.76±2.02 | 60.28±2.17 | 61.14±1.87 | 60.54±2.29 | 60.16±1.68 |
| CSIS | (10) | (100) | (40) | (100) | (100) | (100) | (100) | (100) | (100) | (50) |
| umist | 64.07±1.76 | 61.23±2.15 | 71.71±2.29 | 61.46±2.03 | 56.08 ± 1.80 | 55.43±1.50 | 66.26±1.74 | 64.94±1.65 | 55.88±1.62 | 67.62±1.91 |
| dillist | (10) | (100) | (100) | (70) | (60) | (80) | (100) | (100) | (100) | (70) |
| GLIOMA | 49.59±6.76 | 48.96±3.59 | 34.15±9.10 | 46.51±9.11 | 54.21±2.23 | 45.86±8.08 | 22.01±4.88 | 22.17±5.17 | 21.09±4.65 | 45.14±8.66 |
| GLIONII | (10) | (100) | (50) | (20) | (100) | (20) | (80) | (90) | (100) | (100) |
| pie | 51.01±1.02 | 57.53±0.73 | 57.16±1.01 | 48.05±0.76 | 40.45 ± 0.79 | 50.55±1.03 | 64.94±1.30 | 56.21±0.90 | 65.20±1.42 | 66.66±1.14 |
| pic | (10) | (90) | (70) | (100) | (100) | (100) | (100) | (100) | (100) | (80) |
| LUNG | 63.18±5.48 | 57.44±6.44 | 68.53±5.20 | 63.62±5.41 | 63.74 ± 5.30 | 64.27±5.35 | 67.91±6.23 | 62.23±4.80 | 68.96±5.71 | 72.64±4.69 |
| Lorto | (10) | (70) | (100) | (40) | (90) | (90) | (100) | (20) | (100) | (90) |
| MSTAR | 83.96±3.14 | 73.90±1.62 | 81.85±2.91 | 76.56±1.54 | 78.26 ± 2.51 | 78.18±3.64 | 79.62±2.30 | 78.87±2.52 | 80.53±2.41 | 80.66±2.68 |
| MISTAIN | (10) | (100) | (100) | (100) | (100) | (90) | (100) | (90) | (100) | (100) |
| Average | 65.76±2.98 | 62.16±2.41 | 64.73±3.17 | 60.59±2.96 | 60.13±2.25 | 59.74±2.98 | 62.56±2.66 | 60.64±2.45 | 61.21±2.61 | 67.87±2.97 |

accuracy with a smaller number of selected features makes BSUFS a very practical method for real-world applications.

C. Ablation Experiments

To investigate the effect of bi-sparse regularization terms in BSUFS, this section conducts ablation experiments on

- Case I: BSUFS without $\ell_{2,p}$ -norm and ℓ_q -norm
- Case II: BSUFS without $\ell_{2,p}$ -norm
- Case III: BSUFS without ℓ_q -norm
- Case IV: BSUFS

Note that $p, q \in [0, 1)$.

1) Clustering Efficacy: Table V and Table VI list the clustering performance in terms of ACC and NMI. These results indicate that, except the NMI values on the USPS

and umist datasets, Case IV consistently achieves the top performance for both ACC and NMI metrics. In particular, on the USPS and GLIOMA datasets, the ACC values of Case IV increase from 67.06% to 70.77% and from 49.76% to 61.28% compared to Case I, respectively. In addition, compared with Case III, almost all ACC and NMI results of Case IV are improved, which shows that the introduction of ℓ_q -norm to Case III is meaningful for feature selection.

2) Feature Visualization: Table VII presents visual comparisons of feature selection results of Cases I to IV on the pie dataset. In this study, we set the number of selected features to 80 and randomly select 4 image samples to highlight the effectiveness of feature selection. Although all methods can select the basic facial features (eyes, mouth, nose, lips),

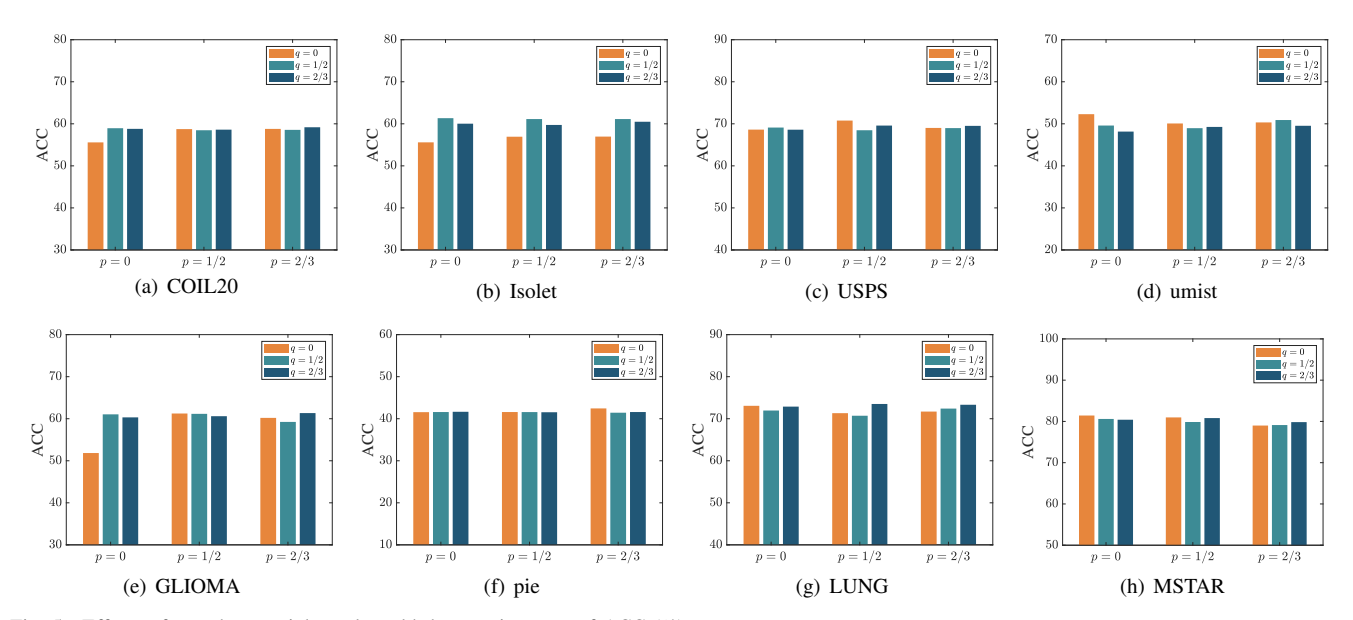


Fig. 5. Effects of p and q on eight real-world datasets in terms of ACC (%).

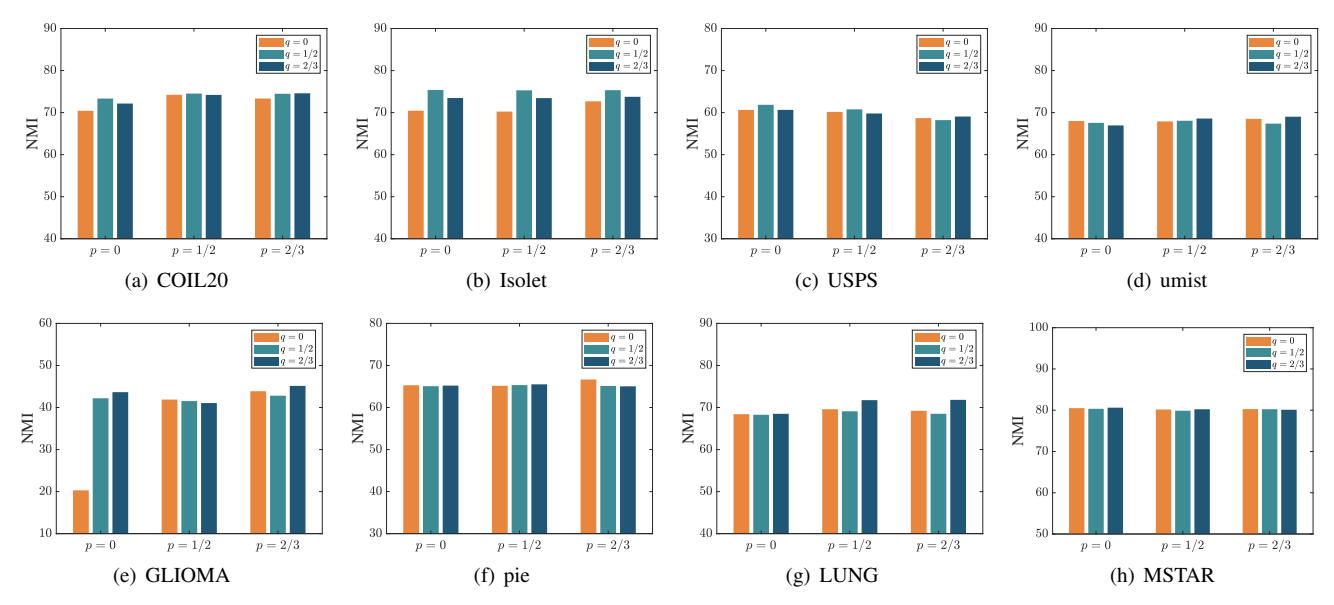


Fig. 6. Effects of p and q on eight real-world datasets in terms of NMI (%).

TABLE V ACC (%) COMPARISONS FOR FOUR CASES IN ABLATION EXPERIMENTS. THE TOP TWO VALUES ARE MARKED AS RED AND BLUE.

| Datasets | Case I | Case II | Case III | Case IV |
|----------|--------|---------|----------|---------|
| COIL20 | 54.09 | 57.19 | 58.76 | 59.18 |
| Isolet | 51.77 | 59.49 | 56.19 | 61.34 |
| USPS | 67.06 | 67.58 | 68.11 | 70.77 |
| umist | 47.16 | 47.52 | 49.23 | 52.29 |
| GLIOMA | 49.76 | 59.16 | 60.12 | 61.28 |
| pie | 40.98 | 40.79 | 41.15 | 42.45 |
| LUNG | 71.34 | 70.30 | 72.33 | 73.51 |
| MSTAR | 79.25 | 78.63 | 80.08 | 81.43 |

TABLE VI
NMI (%) COMPARISONS FOR FOUR CASES IN ABLATION EXPERIMENTS.
THE TOP TWO VALUES ARE MARKED AS RED AND BLUE.

| Datasets | Case I | Case II | Case III | Case IV |
|----------|--------|---------|----------|---------|
| COIL20 | 69.94 | 72.31 | 74.57 | 74.78 |
| Isolet | 66.84 | 73.18 | 72.73 | 75.32 |
| USPS | 60.65 | 59.10 | 61.14 | 60.16 |
| umist | 66.48 | 67.14 | 69.45 | 67.62 |
| GLIOMA | 20.64 | 44.74 | 43.13 | 45.14 |
| pie | 65.02 | 65.13 | 65.23 | 66.66 |
| LUNG | 69.31 | 69.08 | 71.94 | 72.64 |
| MSTAR | 79.92 | 79.61 | 79.97 | 80.66 |

Case IV selects more additional features, such as eyebrows. This diverse selection helps to maintain a more complete

geometric structure of the face, potentially making better use of smaller regions of an image and reducing redundant

TABLE VII

VISUAL COMPARISONS OF SELECTED IMAGE SAMPLES FROM THE PIE DATASET WITH THE CORRESPONDING ACC (%) AND NMI (%).

THE TOP TWO VALUES ARE MARKED AS RED AND BLUE.

| Methods | | Sam | ACC | NMI | | |
|----------|-----------|------------|-----------|------------|-------|-------|
| Case I | thy pain) | the public | The First | the public | 40.98 | 65.02 |
| Case II | 12.00 | A Service | States. | dy jûr | 40.79 | 65.11 |
| Case III | 12.2 | the same | es es | the pure | 41.15 | 65.23 |
| Case IV | 4 | 1 | E VE | 4 | 42.45 | 66.66 |

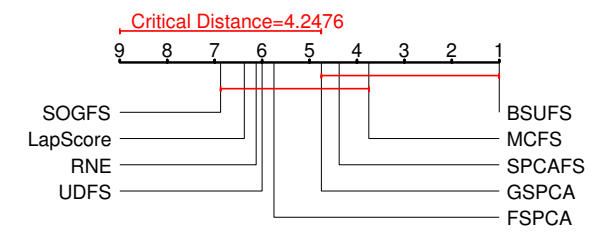


Fig. 7. Post-hoc Nemenyi test of all compared methods.

features. Consequently, Case IV achieves higher ACC and NMI values, which reflects its superior effectiveness.

D. Effects of p and q

There are three common choices of p and q in BSUFS, that are 0, 1/2, and 2/3. In order to evaluate the importance of p and q, Fig. 5 and Fig. 6 present the clustering performance in terms of ACC and NMI under these different values of p and q, respectively. In these two figures, the x-axis represents various values of p and the color variations in the bars indicate different values of q.

According to the clustering results, the following conclusions can be made. First, the optimal choices of p and q are different for different datasets. In specific, for the Isolet dataset, the optimal values of p and q are 0 and 1/2, respectively, while for the LUNG dataset, the optimal values are 1/2 and 2/3, respectively. Second, under different values of p and q, their ACC values and corresponding NMI values are not the same. For example, for the GLIOMA dataset, the ACC value varies greatly at p=0, which also shows that the selection of q also affects the results. Finally, for the umist and MSTAR datasets, the best clustering performance can be observed when both p and q are set to 0, which illustrates that the extension from (0,1) to [0,1) is of importance. However, it needs to be tuned carefully. In practice, it is recommended to determine p first and then q.

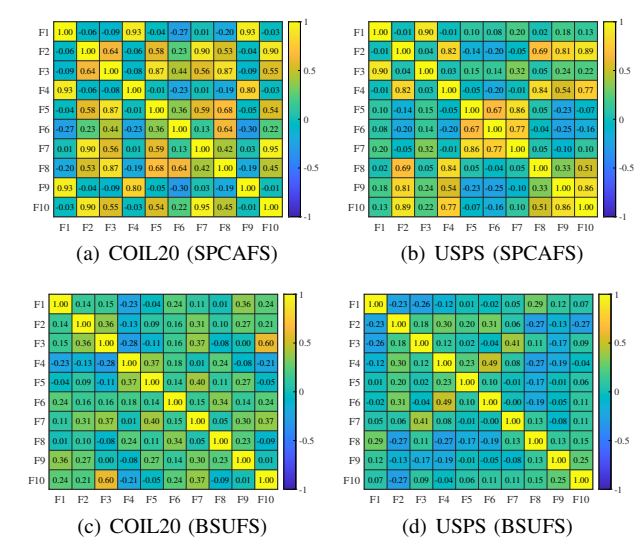


Fig. 8. Heatmap visualizations of correlations for 10 selected features, where (a)-(b) are the results of SPCAFS and (c)-(d) are the results of BSUFS.

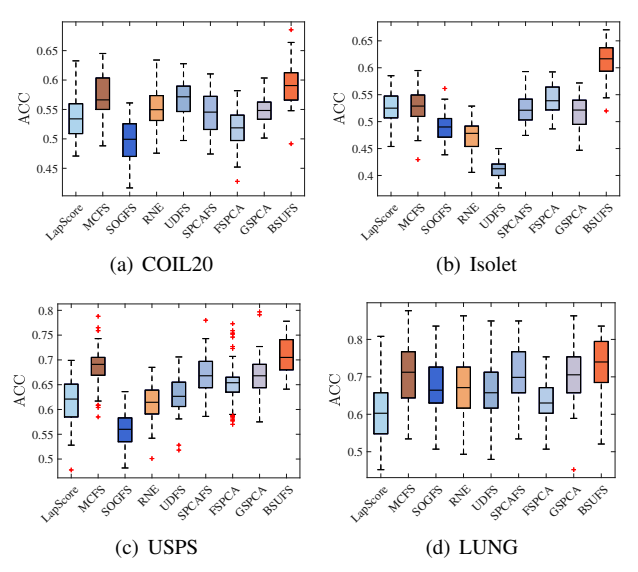


Fig. 9. Model stability comparisons on four selected datasets.

E. Discussion

This section first analyzes statistical tests, then demonstrates the feature correlation differences compared to SPCAFS, and finally from the ACC perspective discusses the model stability, parameter sensitivity, and convergence.

- 1) Statistical Tests: Fig. 7 shows the post-hoc Nemenyi test with the critical difference (CD) value as a metric to evaluate the pairwise differences between compared methods in terms of ACC. It can be found that our proposed BSUFS has statistically significant differences when compared to LapScore, SOGFS, RNE, and UDFS, while no significant differences are observed on the performance of BSUFS relative to MCFS, SPCAFS, and GSPCA.
- 2) Feature Correlation: Fig. 8 shows the feature correlation results using SPCAFS and our proposed BSUFS on the COIL20 and USPS datasets. Here, 10 features are selected, denoted as F_1, F_2, \dots, F_{10} , and the correlation among these

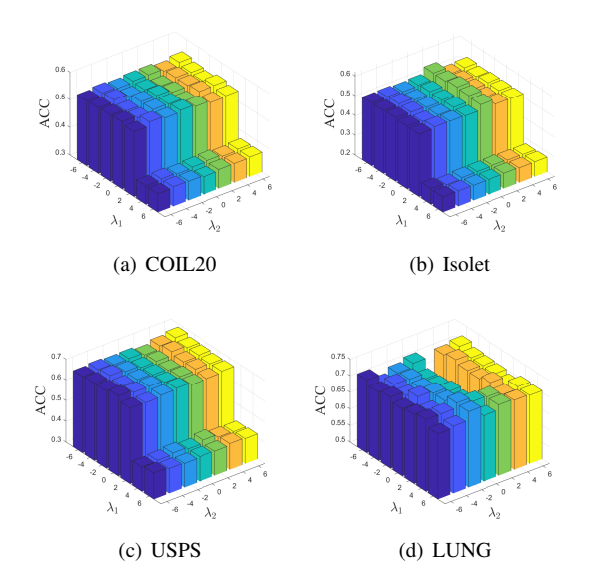


Fig. 10. Parameter sensitivity of λ_1 and λ_2 on four selected datasets.

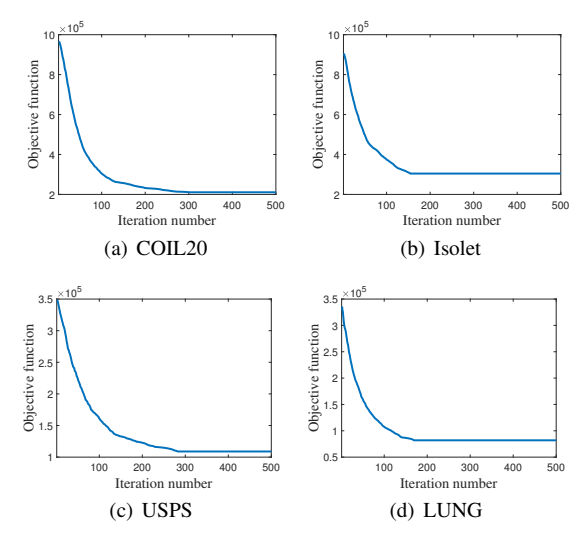


Fig. 11. Convergence curves on four selected datasets.

features are examined. It can be concluded that BSUFS has a smaller feature correlation compared with SPCAFS, indicating that it is very effective in eliminating redundant features.

- 3) Model Stability: In this experiment, box-plots of the 50 clustering results are shown in Fig. 9. It is obvious that in terms of ACC, the average values of BSUFS are generally larger than other methods. Overall, our proposed BSUFS exhibits excellent and stable performance.
- 4) Parameter Sensitivity: Fig. 10 investigates the effects of two regularization parameters, i.e., λ_1 and λ_2 , for the ACC metric. Although the improvement under different λ_2 is not as significant as that under different λ_1 , there are still differences. In general, $\ell_{2,p}$ -norm plays a vital role, while ℓ_q -norm is a complementary choice in feature selection.
- 5) Convergence Analysis: This subsection analyzes the objective value curves in Fig. 11. It can be observed that the objective function of our proposed BSUFS shows a consistent pattern of continuous decrease and reaches stability within

finite iteration numbers. This observation aligns Theorem 3.3 and illustrates the effectiveness of Algorithm 1.

V. CONCLUSION

In this study, a novel method called BSUFS is introduced for UFS, which integrates both $\ell_{2,p}$ -norm and ℓ_q -norm to PCA with $p,q \in [0,1)$. Technically, $\ell_{2,p}$ -norm facilitates feature selection and ℓ_q -norm serves to remove the impact of redundant features. To our best knowledge, it is the first time that models UFS in a unified bi-sparse optimization framework. In algorithms, an efficient PAM optimization scheme is designed and its globally convergent guarantee is also proved rigorously. The feature selection results of BSUFS on synthetic and realworld datasets, respected to ACC and NMI, are more excellent than other competitors. Numerical studies also illustrate that the wide range of p and q is essential, and the best selection of them needs to be determined by the dataset. Furthermore, $\ell_{2,p}$ norm performs a leading role and ℓ_q -norm enhances feature selection. Obviously, this bi-sparse framework can be applied to other related image processing fields.

It should be noted that the sparsity induced by regularization terms requires some tedious and time-consuming parameter selection procedures. In the future, we are interested in applying neural network methodologies [44], [45] to automatically learn parameters and sparse priors.

APPENDIX

For convenience, denote Q = (W, U, V). Then define

$$f(Q) = -\operatorname{Tr}(W^{\top}SW) + \lambda_1 \|V\|_{2,p}^p + \lambda_2 \|U\|_q^q + \frac{\beta_1}{2} \|W - U\|_F^2 + \frac{\beta_2}{2} \|W - V\|_F^2 + \Phi(W).$$
(34)

There are some useful properties for the function f presented in the following lemmas.

Lemma 5.1: The function f(Q) in (34) is proper and lower semicontinuous.

Proof: It is easy to see that the squared Frobenius norm $\|\cdot\|_F^2$ is a continuously differentiable function with a locally Lipschitz continuous gradient. The definitions of $\|\cdot\|_{2,p}^p$ and $\|\cdot\|_q^q$ illustrate that they all are continuous and differentiable. The closeness of the set $\{W\mid W^\top W=I_m\}$ implies that the indicator function $\Phi(W)$ is proper and lower semicontinuous. Therefore, f(Q) is proper lower semicontinuous.

Lemma 5.2: The function f(Q) in (34) satisfies the K-L property at each $Q \in \text{dom } f$.

Proof: As stated in [42], the fact that f(Q) qualifies as a K-L function can be confirmed via each component of f(Q) being a semi-algebraic function. Specifically, the squared Fnorm, $\|\cdot\|_{2,p}^p$, $\|\cdot\|_q^q$, and $\Phi(W)$ are all identified as semi-algebraic functions. Thus, f(Q) satisfies the K-L property at each point of dom f.

The sufficient decrease and relative error conditions of $\{Q^k\}_{k\in\mathbb{N}}$ are proved in the next two lemmas.

Lemma 5.3: Assume the sequence $\{Q^k\}_{k\in\mathbb{N}}$ is generated by Algorithm 1. Then the following inequality holds

$$f(Q^{k+1}) + \tau ||Q^{k+1} - Q^k||_F^2 \le f(Q^k),$$
 (35)

where $\tau = \frac{1}{2} \min\{\tau_1, \tau_2, \tau_3\}.$

Proof: Due to the fact that W^{k+1} , U^{k+1} , and V^{k+1} are optimal solutions of (11), (12), and (13), respectively, the following inequalities hold

$$f(W^{k+1}, U^k, V^k) + \frac{\tau_1}{2} \|W^{k+1} - W^k\|_{\mathrm{F}}^2$$

$$< f(W^k, U^k, V^k),$$
(36)

$$f(W^{k+1}, U^{k+1}, V^k) + \frac{\tau_2}{2} \|U^{k+1} - U^k\|_{\mathsf{F}}^2$$

$$\leq f(W^{k+1}, U^k, V^k),$$
(37)

$$f(W^{k+1}, U^{k+1}, V^{k+1}) + \frac{\tau_3}{2} \|V^{k+1} - V^k\|_{\mathsf{F}}^2$$

$$\leq f(W^{k+1}, U^{k+1}, V^k).$$
(38)

By combining (36)-(38), we have

$$f(W^{k+1}, U^{k+1}, V^{k+1}) + \frac{\tau_1}{2} \|W^{k+1} - W^k\|_{\mathrm{F}}^2$$

$$+ \frac{\tau_2}{2} \|U^{k+1} - U^k\|_{\mathrm{F}}^2 + \frac{\tau_3}{2} \|V^{k+1} - V^k\|_{\mathrm{F}}^2$$

$$\leq f(W^k, U^k, V^k),$$
(39)

which yields

$$f(Q^{k+1}) + \tau ||Q^{k+1} - Q^k||_F^2 \le f(Q^k).$$
 (40)

Hence, the proof is completed.

Lemma 5.4: Assume that $\{Q^k\}_{k\in\mathbb{N}}$ is generated by Algorithm 1. Then, $\{Q^k\}_{k\in\mathbb{N}}$ is bounded. In addition, there exists $V\in\partial f(Q^{k+1})$ such that

$$||V||_{\mathcal{F}} \le a||Q^{k+1} - Q^k||_{\mathcal{F}},\tag{41}$$

where $a = \max\{\tau_1, \beta_1 + \tau_2, \beta_2 + \tau_3\}.$

Proof: First, we prove that $\{Q^k\}_{k\in\mathbb{N}}$ is bounded. Because

$$\lim_{\|W\|_{F} \to +\infty} \Phi(W) = +\infty,$$

$$\lim_{\|U\|_{F} \to +\infty} \frac{\beta_{1}}{2} \|W - U\|_{F}^{2} = +\infty,$$

$$\lim_{\|V\|_{F} \to +\infty} \frac{\beta_{2}}{2} \|W - V\|_{F}^{2} = +\infty,$$
(42)

it is sure that

$$\lim_{\|W\|_{\mathcal{F}} \to +\infty} f(W, U, V) = +\infty,$$

$$\lim_{\|U\|_{\mathcal{F}} \to +\infty} f(W, U, V) = +\infty,$$

$$\lim_{\|V\|_{\mathcal{F}} \to +\infty} f(W, U, V) = +\infty,$$
(43)

which means the function f(Q) would approach infinity if Q is unbounded, *i.e.*, f is coercive. Then the sequence $\{Q^k\}_{k\in\mathbb{N}}$ is bounded if $\{f(Q^k)\}_{k\in\mathbb{N}}$ is finite. According to Lemma 5.3, it holds

$$f(Q^{k+1}) \leq f(Q^{k+1}) + \tau \|Q^{k+1} - Q^k\|_F^2 \leq f(Q^k)$$

$$\leq f(Q^k) + \tau \|Q^k - Q^{k-1}\|_F^2$$

$$\leq \cdots$$

$$\leq f(Q^0),$$
(44)

which leads to a conclusion that $f(Q^{k+1})$ is finite for every k. Therefore, we can conclude that $\{Q^k\}_{k\in\mathbb{N}}$ is bounded.

Following the Karush-Kuhn-Tucker (KKT) conditions of (11), (12), and (13), it has

$$0 \in \partial \Phi(W^{k+1}) - 2SW^{k+1} + \beta_1(W^{k+1} - U^k) + \beta_2(W^{k+1} - V^k) + \tau_1(W^{k+1} - W^k),$$

$$0 \in \partial \lambda_2 \|U^{k+1}\|_q^q + \beta_1(U^{k+1} - W^{k+1}) + \tau_2(U^{k+1} - U^k),$$

$$0 \in \partial \lambda_1 \|V^{k+1}\|_{2,p}^p + \beta_2(V^{k+1} - W^{k+1}) + \tau_3(V^{k+1} - V^k).$$

$$(45)$$

So, there exist $V = (V_1^{k+1}, V_2^{k+1}, V_3^{k+1}) \in \partial f(Q^{k+1})$ with $V_1^{k+1} \in \partial_W f(Q^{k+1}), \ V_2^{k+1} \in \partial_U f(Q^{k+1}), \ \text{and} \ V_3^{k+1} \in \partial_V f(Q^{k+1})$ such that

$$0 = V_1^{k+1} + \tau_1(W^{k+1} - W^k) + \beta_1(U^{k+1} - U^k) + \beta_2(V^{k+1} - V^k), 0 = V_2^{k+1} + \tau_2(U^{k+1} - U^k), 0 = V_3^{k+1} + \tau_3(V^{k+1} - V^k).$$

$$(46)$$

This leads to

$$||V_{1}^{k+1}||_{F} \leq \tau_{1}||W^{k+1} - W^{k}||_{F} + \beta_{1}||U^{k+1} - U^{k}||_{F} + \beta_{2}||V^{k+1} - V^{k}||_{F},$$

$$||V_{2}^{k+1}||_{F} = \tau_{2}||U^{k+1} - U^{k}||_{F},$$

$$||V_{3}^{k+1}||_{F} = \tau_{3}||V^{k+1} - V^{k}||_{F},$$
(47)

which implies that

$$||V||_{F} \le ||V_{1}^{k+1}||_{F} + ||V_{2}^{k+1}||_{F} + ||V_{3}^{k+1}||_{F}$$

$$\le a||Q^{k+1} - Q^{k}||_{F},$$
(48)

where $a = \max\{\tau_1, \beta_1 + \tau_2, \beta_2 + \tau_3\}$. Hence, the desired conclusion is obtained.

Theorem 3.3: Assume $\{(W^k, U^k, V^k)\}_{k \in \mathbb{N}}$ is generated by Algorithm 1. Then, the sequence $\{(W^k, U^k, V^k)\}_{k \in \mathbb{N}}$ globally converges to a critical point of f(W, U, V), i.e.,

$$0 \in \partial f(W^*, U^*, V^*) \tag{49}$$

with $\lim_{k\to +\infty}(W^k,U^k,V^k)=(W^*,U^*,V^*)$ and $\partial f(\cdot)$ being the limiting subdifferential set.

Proof: Now, we have prepared the three required conditions as follows.

- The function f(W, U, V) is proper lower semicontinuous, which has been proved in Lemma 5.1.
- The function f(W, U, V) satisfies the K-L property at each $(W, U, V) \in \text{dom } f$, which has been proved in Lemma 5.2.
- The sequence $\{(W^k,U^k,V^k)\}_{k\in\mathbb{N}}$ satisfies the sufficient decrease and relative error conditions, which have been proved in Lemma 5.3 and Lemma 5.4, respectively.

With any initial point (W^0, U^0, V^0) , suppose the sequence generated by Algorithm 1 is $\{(W^k, U^k, V^k)\}_{k \in \mathbb{N}}$. According to [42], this sequence is convergent to the critical point of f, *i.e.*, there exists a point (W^*, U^*, V^*) such that

$$\lim_{k \to +\infty} (W^k, U^k, V^k) = (W^*, U^*, V^*)$$
 (50)

satisfies $0 \in \partial f(W^*, U^*, V^*)$, which shows the sequence globally converges to a critical point of f. Therefore, the proof is completed.

REFERENCES

- [1] M. I. Jordan and T. M. Mitchell, "Machine learning: Trends, perspectives, and prospects," *Science*, vol. 349, no. 6245, pp. 255–260, 2015.
- [2] R. Zebari, A. Abdulazeez, D. Zeebaree, D. Zebari, and J. Saeed, "A comprehensive review of dimensionality reduction techniques for feature selection and feature extraction," *Journal of Applied Science and Technology Trends*, vol. 1, no. 1, pp. 56–70, 2020.
- [3] V. Bolon-Canedo and B. Remeseiro, "Feature selection in image analysis: a survey," *Artificial Intelligence Review*, vol. 53, no. 4, pp. 2905–2931, 2020.
- [4] Z. Li and J. Tang, "Unsupervised feature selection via nonnegative spectral analysis and redundancy control," *IEEE Transactions on Image Processing*, vol. 24, no. 12, pp. 5343–5355, 2015.
- [5] Z. Hu, J. Wang, K. Zhang, W. Pedrycz, and N. R. Pal, "Bi-level spectral feature selection," *IEEE Transactions on Neural Networks and Learning Systems*, doi: 10.1109/TNNLS.2024.3408208.
- [6] J. C. Ang, A. Mirzal, H. Haron, and H. N. A. Hamed, "Supervised, unsupervised, and semi-supervised feature selection: A review on gene selection," *IEEE/ACM Transactions on Computational Biology and Bioinformatics*, vol. 13, no. 5, pp. 971–989, 2016.
- [7] P. García-Díaz, I. Sánchez-Berriel, J. A. Martínez-Rojas, and A. M. Diez-Pascual, "Unsupervised feature selection algorithm for multiclass cancer classification of gene expression rna-seq data," *Genomics*, vol. 112, no. 2, pp. 1916–1925, 2020.
- [8] M. M. Rahman, O. L. Usman, R. C. Muniyandi, S. Sahran, S. Mohamed, and R. A. Razak, "A review of machine learning methods of feature selection and classification for autism spectrum disorder," *Brain Sciences*, vol. 10, no. 12, p. 949, 2020.
- [9] J. Cai, J. Luo, S. Wang, and S. Yang, "Feature selection in machine learning: A new perspective," *Neurocomputing*, vol. 300, pp. 70–79, 2018.
- [10] J. G. Dy and C. E. Brodley, "Feature selection for unsupervised learning," *Journal of Machine Learning Research*, vol. 5, no. Aug, pp. 845–889, 2004.
- [11] Y. Guo, Y. Zhang, Y. Chen, and S. X. Yu, "Unsupervised feature learning with emergent data-driven prototypicality," in *Proceedings of* the IEEE/CVF Conference on Computer Vision and Pattern Recognition, 2024, pp. 23199–23208.
- [12] S. Solorio-Fernández, J. A. Carrasco-Ochoa, and J. F. Martínez-Trinidad, "A review of unsupervised feature selection methods," *Artificial Intelligence Review*, vol. 53, no. 2, pp. 907–948, 2020.
- [13] Q. Zhou, Q. Wang, Q. Gao, M. Yang, and X. Gao, "Unsupervised discriminative feature selection via contrastive graph learning," *IEEE Transactions on Image Processing*, vol. 33, pp. 972–986, 2024.
- [14] D. Shi, L. Zhu, J. Li, Z. Zhang, and X. Chang, "Unsupervised adaptive feature selection with binary hashing," *IEEE Transactions on Image Processing*, vol. 32, pp. 838–853, 2023.
- [15] X. He, D. Cai, and P. Niyogi, "Laplacian score for feature selection," in *Advances in Neural Information Processing Systems*, vol. 18, 2005, pp. 507–514.
- [16] D. Cai, C. Zhang, and X. He, "Unsupervised feature selection for multicluster data," in *Proceedings of the 16th ACM SIGKDD International Conference on Knowledge Discovery and Data Mining*, 2010, pp. 333– 342.
- [17] Y. Yang, H. T. Shen, Z. Ma, Z. Huang, and X. Zhou, "\(\ell_{2,1}\)-norm regularized discriminative feature selection for unsupervised learning," in *IJCAI International Joint Conference on Artificial Intelligence*, 2011, pp. 1589–1594.
- [18] F. Nie, W. Zhu, and X. Li, "Unsupervised feature selection with structured graph optimization," in *Proceedings of the AAAI Conference* on Artificial Intelligence, vol. 30, no. 1, 2016.
- [19] Y. Liu, D. Ye, W. Li, H. Wang, and Y. Gao, "Robust neighborhood embedding for unsupervised feature selection," *Knowledge-Based Systems*, vol. 193, p. 105462, 2020.
- [20] J. Li, K. Cheng, S. Wang, F. Morstatter, R. P. Trevino, J. Tang, and H. Liu, "Feature selection: A data perspective," ACM Computing Surveys, vol. 50, no. 6, pp. 1–45, 2017.
- [21] M. Greenacre, P. J. Groenen, T. Hastie, A. I. d'Enza, A. Markos, and E. Tuzhilina, "Principal component analysis," *Nature Reviews Methods Primers*, vol. 2, no. 1, p. 100, 2022.
- [22] H. Zou and L. Xue, "A selective overview of sparse principal component analysis," *Proceedings of the IEEE*, vol. 106, no. 8, pp. 1311–1320, 2018.
- [23] Z. Li, F. Nie, J. Bian, D. Wu, and X. Li, "Sparse PCA via $\ell_{2,p}$ -norm regularization for unsupervised feature selection," *IEEE Transactions*

- on Pattern Analysis and Machine Intelligence, vol. 45, no. 4, pp. 5322–5328, 2023.
- [24] L. Tian, F. Nie, R. Wang, and X. Li, "Learning feature sparse principal subspace," *Advances in Neural Information Processing Systems*, vol. 33, pp. 14 997–15 008, 2020.
- [25] X. Zhang, J. Zheng, D. Wang, G. Tang, Z. Zhou, and Z. Lin, "Structured sparsity optimization with non-convex surrogates of ℓ_{2,0}-norm: A unified algorithmic framework," *IEEE Transactions on Pattern Analysis and Machine Intelligence*, vol. 45, no. 5, pp. 6386–6402, 2023.
- [26] Y. Hu, C. Li, K. Meng, J. Qin, and X. Yang, "Group sparse optimization via $\ell_{p,q}$ regularization," *Journal of Machine Learning Research*, vol. 18, no. 30, pp. 1–52, 2017.
- [27] Y. Tian and Y. Zhang, "A comprehensive survey on regularization strategies in machine learning," *Information Fusion*, vol. 80, pp. 146– 166, 2022.
- [28] Y. Zhu, X. Zhang, G. Wen, W. He, and D. Cheng, "Double sparse-representation feature selection algorithm for classification," *Multimedia Tools and Applications*, vol. 76, pp. 17525–17539, 2017.
- [29] H. Wang, F. Nie, H. Huang, S. L. Risacher, A. J. Saykin, L. Shen, and A. D. N. Initiative, "Identifying disease sensitive and quantitative trait-relevant biomarkers from multidimensional heterogeneous imaging genetics data via sparse multimodal multitask learning," *Bioinformatics*, vol. 28, no. 12, pp. i127–i136, 2012.
- [30] H. Wang, F. Nie, and H. Huang, "Multi-view clustering and feature learning via structured sparsity," in *International Conference on Machine Learning*. PMLR, 2013, pp. 352–360.
- [31] R. Rubinstein, M. Zibulevsky, and M. Elad, "Double sparsity: Learning sparse dictionaries for sparse signal approximation," *IEEE Transactions* on Signal Processing, vol. 58, no. 3, pp. 1553–1564, 2010.
- [32] X. Bian, W. Xu, and S. Wang, "Double-sparsity recovery for addistorted compressive sensing," in 2022 IEEE 33rd Annual International Symposium on Personal, Indoor and Mobile Radio Communications (PIMRC). IEEE, 2022, pp. 1215–1220.
- [33] Y. Hu, J.-X. Liu, Y.-L. Gao, and J. Shang, "Dstpca: Double-sparse constrained tensor principal component analysis method for feature selection," *IEEE/ACM Transactions on Computational Biology and Bioinformatics*, vol. 18, no. 4, pp. 1481–1491, 2021.
- [34] S. Zhang, Y. Liu, and X. Li, "Micro-doppler effects removed sparse aperture isar imaging via low-rank and double sparsity constrained ADMM and linearized ADMM," *IEEE Transactions on Image Process*ing, vol. 30, pp. 4678–4690, 2021.
- [35] Z. Li, J. Liu, Y. Yang, X. Zhou, and H. Lu, "Clustering-guided sparse structural learning for unsupervised feature selection," *IEEE Transac*tions on Knowledge and Data Engineering, vol. 26, no. 9, pp. 2138– 2150, 2014.
- [36] P. Jain, P. Kar et al., "Non-convex optimization for machine learning," Foundations and Trends® in Machine Learning, vol. 10, no. 3-4, pp. 142–363, 2017.
- [37] S. Zhou, "Sparse SVM for sufficient data reduction," *IEEE Transactions on Pattern Analysis and Machine Intelligence*, vol. 44, no. 9, pp. 5560–5571, 2022.
- [38] J. Bai, L. Jia, and Z. Peng, "A new insight on augmented lagrangian method with applications in machine learning," *Journal of Scientific Computing*, vol. 99, no. 2, p. 53, 2024.
- [39] P.-A. Absil, R. Mahony, and R. Sepulchre, Optimization Algorithms on Matrix Manifolds. Princeton University Press, 2008.
- [40] S. Zhou, X. Xiu, Y. Wang, and D. Peng, "Revisiting $L_q (0 \le q < 1)$ norm regularized optimization," arXiv:2306.14394, 2023.
- [41] H. Attouch, J. Bolte, and B. F. Svaiter, "Convergence of descent methods for semi-algebraic and tame problems: Proximal algorithms, forward– backward splitting, and regularized gauss–seidel methods," *Mathemati*cal Programming, vol. 137, no. 1, pp. 91–129, 2013.
- [42] J. Bolte, S. Sabach, and M. Teboulle, "Proximal alternating linearized minimization for nonconvex and nonsmooth problems," *Mathematical Programming*, vol. 146, no. 1, pp. 459–494, 2014.
- [43] Z. Xu, X. Chang, F. Xu, and H. Zhang, "\(\ell_{1/2}\) regularization: A thresholding representation theory and a fast solver," *IEEE Transactions on Neural Networks and Learning Systems*, vol. 23, no. 7, pp. 1013–1027, 2012.
- [44] T. Chen, X. Chen, W. Chen, H. Heaton, J. Liu, Z. Wang, and W. Yin, "Learning to optimize: A primer and a benchmark," *Journal of Machine Learning Research*, vol. 23, no. 189, pp. 1–59, 2022.
- [45] J. Zhang, B. Chen, R. Xiong, and Y. Zhang, "Physics-inspired compressive sensing: Beyond deep unrolling," *IEEE Signal Processing Magazine*, vol. 40, no. 1, pp. 58–72, 2023.